AGU ADVANCING EARTH AND SPACE SCIENCES

Hydrous Regions of the Mantle Transition Zone Lie Beneath Areas of Continental Intraplate Volcanism

Helene Wang[1,2] , Valentina Magni[1,3] , Clinton P. Conrad[1,4] , and Mathew Domeier[1,4]

[1]Centre for Earth Evolution and Dynamics (CEED), University of Oslo, Oslo, Norway, [2]TGS, Oslo, Norway, [3]Norwegian Geotechnical Institute (NGI), Oslo, Norway, [4]Centre for Planetary Habitability (PHAB), University of Oslo, Oslo, Norway

Abstract Great volumes of water are carried downward into the mantle transition zone (MTZ, 410–670 km depth) by subducting slabs. If this water is later drawn upward, the resulting mantle melting may generate continental intraplate volcanism (IPV). Despite water's importance, its amount and spatial distribution within the MTZ, and its impact on IPV, are poorly constrained. Here we use plate tectonic reconstructions to estimate the rates and positions of water injection into the MTZ by subducted slabs during the past 400 Myr. This allows us to construct global maps of heterogeneous MTZ hydration, which we then compare to IPV eruption locations from the past 200 Myr. We detect a statistically significant correlation between wet MTZ regions and IPV locations at the surface, but only if slabs sink faster than 1 cm/yr, water remains stored in the MTZ for periods of 30–100 Myr, and IPV eruptions occur 10–30 Myr later. We find that 42%–68% of continental IPV is underlain by wet MTZ, with greater fractions associated with longer MTZ residence time. Hydrous underpinning of continental IPV was highest during the Jurassic, when more extensive slab interaction with the MTZ hydrated a wider area of the MTZ. Since the Cretaceous, continents have been moving over the wet MTZ, increasing IPV possibilities. MTZ regions near the northern Pacific, southern Africa, and western Europe have remained dry by avoiding wet slabs. We suggest that subducted water shapes global patterns of intraplate volcanism, with hydrous upwellings rising from the MTZ to generate continental IPV above wet MTZ regions.

Plain Language Summary Minerals within the Earth's interior may hold several oceans of water. Most of this water is stored within the mantle transition zone (MTZ), a layer that lies between 410 and 670 km in depth. It is carried there by subducted "slabs," which are tectonic plates that have descended into the mantle. We used reconstructions of past plate motions to determine the locations and rates of water transport into the MTZ by slabs during the past 400 million years. This exercise allows us to construct maps of water storage within Earth's MTZ. These maps suggest that more than a third of the MTZ is likely to be hydrated today, and even greater areas were hydrated in the past. We also found that "intraplate" volcanism, which erupts away from tectonic plate boundaries, tends to preferentially occur above these "wet" areas of the MTZ, especially if water remains in the MTZ for long periods of time. Based on this correlation, we suggest that MTZ hydration exerts an important control on global patterns of intraplate volcanism. This occurs via hydrous upwellings that carry water and heat upward from the MTZ. Near the surface, these upwellings increase the tendency of rocks to melt and form magma that can erupt.

1. Introduction

Water exchange between the Earth's surface and interior is facilitated by active plate tectonic processes, primarily subduction and mid-ocean ridge volcanism (Figure 1) (e.g., Bodnar et al., 2013; Thompson, 1992). The process of transporting water from the surface into the mantle through subduction is known as regassing (Figure 1) (Rüpke et al., 2004; Syracuse et al., 2010), and regassing rates depend on many parameters that control the thermal structure of subducting slabs. Old and fast slabs have a greater capacity to transport water to great depths (ca. >200 km) than young and warm, slowly subducting slabs (Thompson, 1992; van Keken et al., 2011). This is mainly because the old and thick lithosphere that subducts rapidly can maintain a cold interior for longer, which allows hydrous phases within the slab to remain stable to greater depths. Water that reaches the mantle transition zone (MTZ, between 410 and 670 km depth) can be stored there for long periods within the minerals ringwoodite and wadsleyite (Hirschmann, 2006; Karato et al., 2020), especially if the slab's passage through the MTZ is slowed by slab stagnation, deformation, or horizontal deflection (Komabayashi & Omori, 2006; Kuritani et al., 2011; Ohtani et al., 2018; Suetsugu et al., 2006). The presence of water within the MTZ has been confirmed by examination of mineral inclusions within sublithospheric diamonds (Pearson et al., 2014; Shirey et al., 2021;

Wirth et al., 2007), and isotopic evidence suggests that MTZ water may have been recycled from the surface environment (Xing et al., 2024). Because slabs on Earth exhibit a diversity of thicknesses and descent rates, the subduction-mediated processes that deliver water to the deep mantle (>200 km, beyond extraction by volcanic arcs, see Figure 1) are highly variable in space and time (e.g., Karlsen et al., 2019; van Keken et al., 2011). Thus, even though the MTZ may hold even more water than Earth's surface environment (e.g., Nestola & Smyth, 2016), the distribution of this water within the MTZ may be highly heterogeneous (Peslier et al., 2017).

Characterizing the water content of the transition zone is important because it can help us to understand Earth's deep mantle water cycle, which regulates mantle convection (e.g., Karato, 2011), upper mantle rheology (e.g., Ramirez et al., 2022), volcanic processes (e.g., Yang & Faccenda, 2020), Phanerozoic sea level (e.g., Karlsen et al., 2019), and Earth's thermal evolution (e.g., Crowley et al., 2011). However, detecting variations in MTZ hydration has proven difficult because such variations do not significantly influence seismic wave speeds (Schulze et al., 2018). Instead, variations in water content have been inferred from observations of transition zone thickness (Houser, 2016; Meier et al., 2009; Suetsugu et al., 2006), seismic anisotropy (Chang & Ferreira, 2019), seismic attenuation (Zhu et al., 2013), reflections or conversions from layers of dehydration melt products (Hier-Majumder & Tauzin, 2017; Schmandt et al., 2014), and electrical conductivity (Huang et al., 2005; Karato, 2011; Kelbert et al., 2009). The interpretation of such variations in terms of hydration heterogeneity may be complicated by the presence of other heterogeneities (e.g., temperature or composition (e.g., Ramirez et al., 2022)), as suggested by conflicting inferences of mostly wet (Kelbert et al., 2009) or mostly dry (Chang & Ferreira, 2019) conditions near subducting slabs. Overall, the magnitude and distribution of water in the Earth's interior, both today and in the geologic past, remain poorly quantified and mapped (Hirschmann, 2006).

One indicator of a hydrated MTZ may be intraplate volcanism (IPV), defined as volcanism occurring within the interiors of tectonic plates, that is, away from plate boundaries. Although a few locations of vigorous IPV can be linked to deep mantle plumes (e.g., Hawaii), the source for most areas of IPV remains enigmatic (e.g., Courtillot et al., 2003). Some IPV locations may also result from a variety of sub-lithospheric processes, including shear-driven upwelling (e.g., Ballmer et al., 2015; Conrad et al., 2011), lithospheric deformation (e.g., Valentine & Hirano, 2010), and small-scale convective instability (e.g., Ballmer et al., 2010; King & Ritsema, 2000). These IPV mechanisms rely on decompression melting beneath the lithosphere (e.g., Aivazpourporgou et al., 2015; Hernlund et al., 2008), which can be enhanced if the solidus temperature is depressed by the presence of water (Katz et al., 2003). Because a variety of different local-scale processes have been proposed to explain disparate IPV eruptions both past and present, it is difficult to contextualize IPV within a globally unifying framework.

Some non-plume IPV has been linked to the mantle transition zone (Courtillot et al., 2003), and especially above mantle slabs that have stagnated there (e.g., Kameyama & Nishioka, 2012; Kuritani et al., 2011). The mechanism for such IPV has also remained enigmatic, but several authors have noted that the negative buoyancy of hydrous minerals in the MTZ (e.g., Inoue et al., 2004; Panero, 2010) could generate gravitational instabilities within the hydrated parts of the MTZ (e.g., Kuritani et al., 2019; Motoki & Ballmer, 2015; Richard & Bercovici, 2009). Such instabilities may manifest as "hydrous upwellings" that rise from an MTZ water reservoir (e.g., Long et al., 2019; Yang & Faccenda, 2020). Because minerals found above the MTZ can bear less water, the upward flux of hydrated mantle above the 410 km discontinuity would result in hydrous melting (Karato et al., 2020; X.-C. Wang et al., 2015) and possibly the upward transport of melt before eruption at the surface (Figure 1). This link between IPV and a hydrated MTZ may explain Cenozoic IPV in a few continental locations such as Northeast China (Kuritani et al., 2019; Yang & Faccenda, 2020), where the Pacific slab has stagnated in the MTZ for more than 30 Myr. Despite such local case studies for specific IPV fields, we lack a global context for understanding IPV in terms of upwelling or other processes linked to the hydrated MTZ.

In this study, we look for a possible global connection between continental intraplate volcanism and hydrated regions of the mantle transition zone. To achieve this, we use global plate tectonic reconstructions to predict patterns of heterogeneous water storage in the MTZ during the past 400 Myr (Section 2.1). We then test to see if continental IPV locations, inferred from a geochemical database (Section 2.2), preferentially erupt above the more hydrated regions of the MTZ (Section 2.3). Because our estimates of both subduction history and IPV patterns are imperfect, especially for earlier times, we examine geographical correlations between the MTZ hydration state and IPV eruption locations across all continental areas (Section 3). This allows us to use statistical correlation methods to quantify any inferred link between IPV locations and the hydrated MTZ (Section 4).
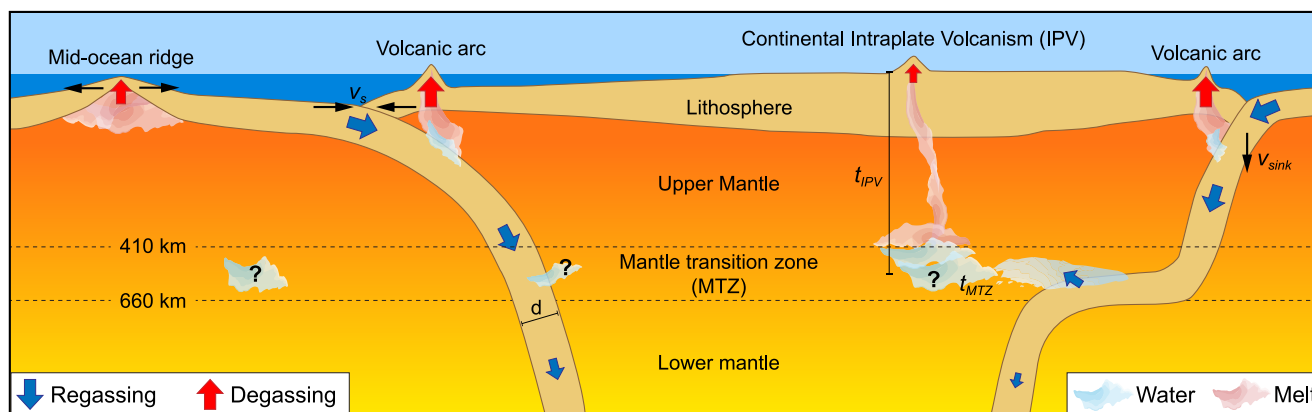
Figure 1. Schematic of the deep Earth water cycle. Water exchange between Earth's surface and deep interior is controlled by plate tectonics. Degassing releases water into the surface environment at spreading ridges, arc volcanoes, and through intraplate volcanism (IPV). Regassing transport water back into the deep mantle via subduction with velocity v_{sink}. Most of a slab's initial water is released in the mantle wedge, where it triggers partial melting and is degassed to the surface through arc volcanism. The remaining water is transported beyond the arc and can be released within the mantle transition zone (MTZ), where slabs often stagnate. More water reaches the MTZ for subduction zones with a larger convergence velocity (v_s) and a greater slab age (which determines the slab thickness, d). Water is plausibly stable within the MTZ for a significant time (t_{MTZ}), possibly even after the slab has continued sinking into the lower mantle. The hydrous MTZ may induce hydrous upwelling, melting, and subsequent IPV that is not plume-related (e.g., Yang & Faccenda, 2020). Eruptions at continental intraplate locations above water-rich parts of the MTZ could occur after an unknown delay period (t_{IPV}) following MTZ hydration.

2. Methods

Because the mechanisms for both hydration of the MTZ and eruption of IPV at the surface are poorly understood, we develop several alternative models of MTZ hydration based on values of key parameters whose true values are unknown. We then compare patterns of predicted MTZ hydration with continental IPV locations, compiled as described below, in order to discover any links between them.

2.1. Predictive Maps of Hydrated Regions Within the Mantle Transition Zone

To construct maps of the hydrated portions of the MTZ, we used the global plate tectonic model of Matthews et al. (2016) with corrections for the Pacific described by Torsvik et al. (2019). The plate model is constructed upon a mantle-based absolute reference frame, extends from 410 Ma to present-day, and is accompanied by seafloor ages computed by Karlsen et al. (2021) (Figure 2, left column). For each 1 Myr time step, we extract the coordinates of the subduction zone segments, as well as their convergence velocity (v_s), length (L_s), and slab age (τ), all of which vary spatially and with time during the past 400 Myr (Figure S1 in Supporting Information S1). We use these parameters to estimate the flux of water into the deep mantle for each subduction zone segment at each time step, following the parametrization of Karlsen et al. (2019) (see Text S1 in Supporting Information S1). The resulting regassing rates vary along and among Earth's different subduction zones (Figure 2, left column), and global rates of net regassing into the deep mantle exhibit significant temporal variations (Figure S1e in Supporting Information S1). These regassing rates can be used to reconstruct hydration patterns in the MTZ as a function of time. The simplest way to do this is to integrate the historical water flux (HWF) for surface subduction zones for a chosen period of time. HWF is computed for each reconstruction age as the mass of along-trench regassed water that could have accumulated within the MTZ. By assuming an accumulation period (e.g., 100 Myr) we can predict patterns of MTZ hydration that can be compared to the observed history of continental IPV (Figure 2, right column).

We convert integration of HWF (units of Tg per meter of trench length, right column of Figure 2) into maps of MTZ hydration density (kg of water per square km of MTZ), which are more useful for comparing to continental IPV eruptions. For this, we express regassing fluxes at subduction zones on a mesh of 10,094 nodes distributed with relatively uniform spacing (∼225 km at the surface) over a sphere (Figure S2 in Supporting Information S1). This results in a mapping of the water flux from the surface into the mantle at a particular time. We assume that water subducts vertically downward into the mantle beneath trench segment midpoints with a constant sinking velocity v_{sink}, which allows us to translate the water flux map to a specific mantle depth. Average upper mantle sinking velocities of 1–4 cm/yr (van der Meer et al., 2018), 1.5–6.0 cm/yr (Domeier et al., 2016), 5–7 cm/yr (Goes
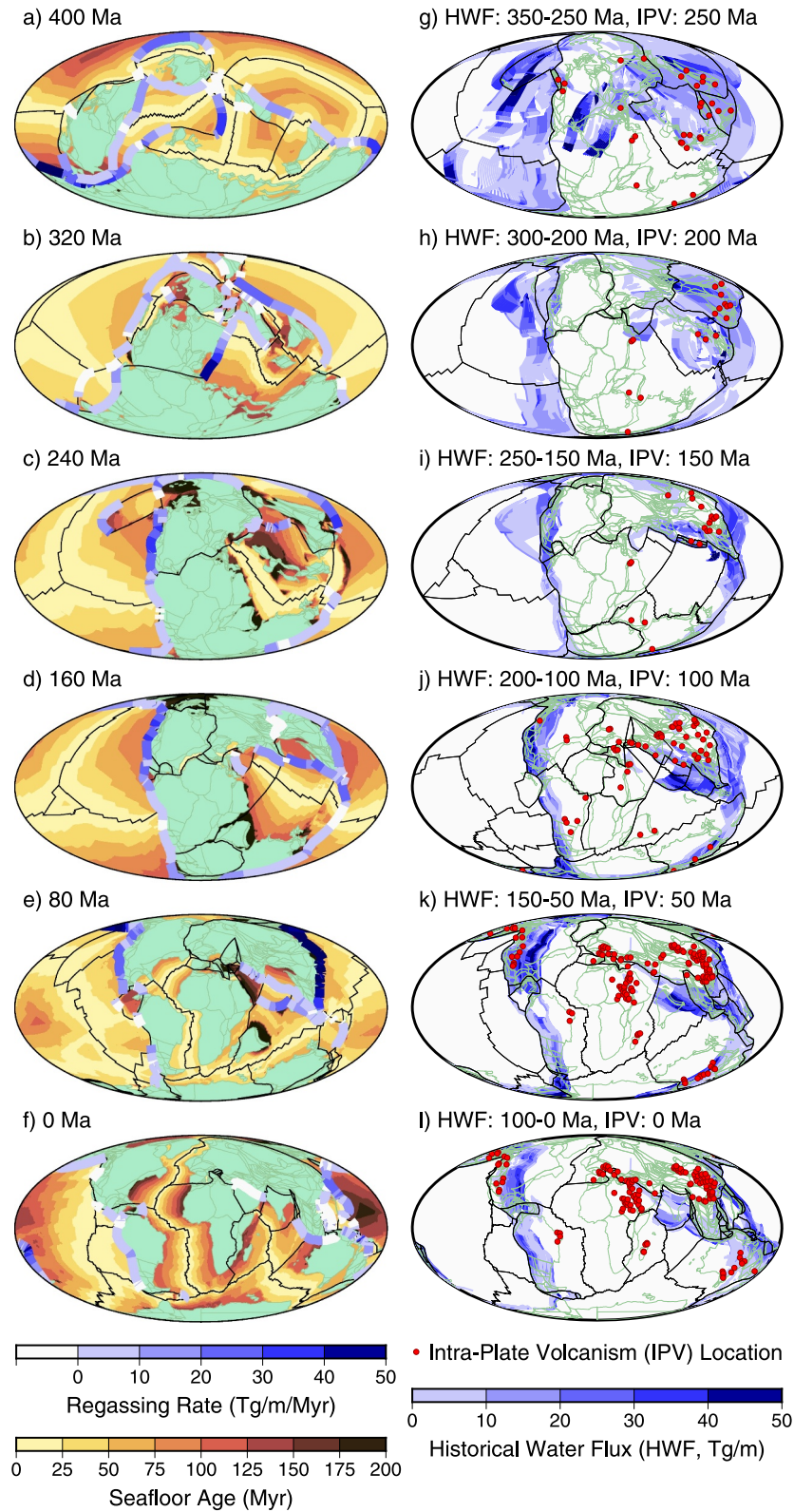
Figure 2.

et al., 2011), and 10 cm/yr (Bercovici & Karato, 2003) have been suggested. Here, we employ v_{sink} as an unknown parameter and examine values in the range of 1–9 cm/yr above 660 km depth.

As they encounter the lower mantle, slabs are thought to slow down (e.g., Butterworth et al. (2014) estimated sinking rates of 1.3 cm/yr in the lower mantle), a process that may already begin in the MTZ. Some slabs appear to penetrate through the MTZ, whereas other slabs stagnate there for a period of time (Figure 1 (Goes et al., 2017)). For scenarios of slab stagnation, we apply a sinking rate of 0 cm/yr at the 660 km discontinuity for a time t_{MTZ}, which we refer to as the MTZ residence time. We note that the effective MTZ residence time may be longer than the time that slabs actually stagnate in the MTZ. This is because any water that is released from a stagnating slab can be stored within wadsleyite and ringwoodite in the MTZ, even after the slab itself has moved deeper into the mantle. Because the duration of slab stagnation is unknown, we employ t_{MTZ} as another unknown parameter and examine plausible scenarios that include t_{MTZ} of 0, 30, and 100 Myr, after which we remove this water from the MTZ. We also consider an "infinite" end member case, named $t_{MTZ} = \infty$, in which all regassed water that reaches the MTZ stays there until the end of the simulation.

Within the upper mantle, water in the slab may diffuse into surrounding minerals (Demouchy & Bolfan-Casanova, 2016) where migration relative to the solid flow can increase the lateral reach of the subducted water (Hebert & Montési, 2013). In addition to diffusion, the location of the water may deviate from the surface location of the trench because slabs dip and deform as they descend, and may drift horizontally if they stagnate (Goes et al., 2017). To account for the lateral movement of water after subduction as well as uncertainties related to reconstructed subduction zone locations, we distribute water from each subduction zone segment into the N closest neighbor mesh points that surround the segment midpoint, with closer points getting more water (Text S2 in Supporting Information S1). We use $N = 10$, which distributes the water within a radius of about 390 km of the segment midpoint (Figure S2 in Supporting Information S1) and is consistent with slow diffusion and migration processes (Demouchy & Bolfan-Casanova, 2016; Hebert & Montési, 2013). Sensitivity experiments show that increasing N has only a modest effect on the water distribution within the MTZ (Text S2 in Supporting Information S1). Instead, the lateral coverage of water in the MTZ is more closely related to slab stagnation (Section 3.2 below). This is because slab stagnation retains water within the MTZ while subduction locations, and thus MTZ injection points, dictate its distribution. The largest control on the lateral extent of MTZ hydration is thus exerted by the MTZ residence time t_{MTZ}.

2.2. Location of Continental Intraplate Volcanism

To identify locations of continental intraplate volcanism (IPV), we selected all onshore basalts classified as "Intraplate Volcanism" from the GEOROC (Geochemistry of Rocks of the Oceans and Continents, https://georoc.eu/) database (Lehnert et al., 2000) with assigned eruption ages within the most recent 250 Myr. The choice of 250 Myr allows time for the tectonic reconstruction to populate the MTZ with water following the start of the tectonic reconstruction at 410 Ma.

Compared to continents, oceanic regions host more extensive intraplate volcanism (Heyn & Conrad, 2022), making them a potentially rich source of information about intraplate volcanism patterns. However, we do not know eruption ages for most of the thousands of seamounts that have been detected across the ocean basins (Gevorgian et al., 2023). This presents a challenge to reconstruct their eruption locations in order to compare them with the lateral extent of the wet MTZ. Furthermore, the fact that intraplate volcanism is so much more extensive in the ocean basins makes detecting spatial patterns difficult beyond volumetric comparisons between basins or as a function of seafloor age (Conrad et al., 2017). For these reasons, we did not consider intraplate volcanism

Figure 2. Regassing rates for subduction zone segments (left column) colored according to the amount of water per unit length of subduction zone segment (per Myr) at (a) 400 Ma, (b) 320 Ma, (c) 240 Ma, (d) 160 Ma, (e) 80 Ma, and (f) 0 Ma (present day). Subduction zone segments that do not contribute to the deep mantle water flux (because they are too warm or subduct too slowly) are displayed as white segments. Also shown for context are reconstructed seafloor ages (colors in oceanic regions, from Karlsen et al. (2019)), plate boundaries (black lines), and continental blocks (green regions). **Historical water flux (HWF) and continental intraplate volcanism (IPV) eruption locations (right column)** are shown at (g) 250 Ma, (h) 200 Ma, (i) 150 Ma, (j) 100 Ma, (k) 50 Ma, and (l) 0 Ma (present-day). Here HWF (colors) represents the mass of water (per unit trench length) that has been injected into the deep mantle by subduction during the previous 100 Myrs (plotted using 1 Myr intervals). Our analysis compares representations of HWF to observed continental IPV locations, which are shown by red circles (see text for how IPV locations are determined).

locations within oceanic areas, and we excluded sites in the GEOROC database that are classified as ocean islands.

Although some of the continental IPV points in the data set are likely related to plumes with a deep mantle source below the MTZ, we did not attempt to remove such points because it is difficult to distinguish plume-associated IPV from other IPV. Thus, we used the database "as-is" (downloaded on 16 November 2021) to avoid selection bias. Importantly, the database shows only the present-day location of IPV, but due to plate motions, most of these sites were in a different location at the time of their emplacement. Therefore, we computed the original position of each IPV point according to the same plate reconstruction model used to estimate the water flux into the mantle (Matthews et al., 2016; Torsvik et al., 2019), yielding maps of continental IPV locations for past times (Figure 2, right column). For comparison to MTZ hydration, we also filtered the data to exclude duplicate points and merged clustered points to mitigate oversampling (Text S3 and Figure S3 in Supporting Information S1).

2.3. Occurrence of IPV Above Wet or Dry Mantle

Having developed models for MTZ hydration and continental IPV eruption as a function of time and space (Figure 2), we now seek to determine if there exists any meaningful correlation between them. We might anticipate a delay period (t_{IPV}) representing the time it takes for water stored in the MTZ to induce eruption of IPV at the surface. This time may be associated with extraction of hydrous material from the slab (e.g., Richard & Bercovici, 2009), ascent of hydrous upwellings from the MTZ, and melt transit through the lithosphere. Previous studies have suggested IPV delay periods of ~12 Myr (Yang & Faccenda, 2020), tens of Myr (Motoki & Ballmer, 2015), and 10–30 Myr (Long et al., 2019). Therefore, we compare IPV maps (e.g., Figure 2, right column) with MTZ hydration maps that are older by t_{IPV} delay periods of 0, 10, 20, 30, and 50 Myr.

We interpolate our MTZ hydration models (Section 2.1) to determine the concentration of water in the MTZ beneath each IPV point. To identify regions of the MTZ where subducted water may have accumulated, we choose a threshold of $0.5 \cdot 10^9$ kg/km^2 for the "wet mantle transition zone," while values below this cutoff are designated as "dry." This threshold lies just above the minimum non-zero MTZ water content in our maps (e.g., Figure 3) and is ~17 times smaller than the 0.001 wt% cutoff used by Zhang et al. (2022) to define the "dry" MTZ. We note, however, that the water content of the MTZ is unlikely to be distributed uniformly because water is delivered to the MTZ heterogeneously by narrow regions within the slab that escape dehydration on their way to the MTZ (van Keken et al., 2011). If embedded within a 5 km layer within a stagnant slab, our minimum threshold for MTZ water ($0.5 \cdot 10^9$ kg/km^2) equates to a water concentration of 30 wt.-ppm water, which is sufficient to depress the sublithospheric solidus by several km (Hirschmann, 2006; Katz et al., 2003) and potentially promote IPV. Water concentrations about an order of magnitude larger in parts of the MTZ have been shown to generate hydrous upwelling leading to sublithospheric melting (Long et al., 2019), but the minimum water content needed to potentially drive hydrous upwelling is not known. We have thus used a conservative low value for the "wet" MTZ threshold that, combined with our choices for distributing subducted water onto the MTZ grid (Text S2 in Supporting Information S1), incorporates some degree of uncertainty associated with lateral movement of water in the MTZ. Our wet/dry distinction thus attempts to identify all regions of the MTZ that may have retained any water from the slabs. Finally, we note that the specific choice of a threshold may not be particularly important, because the area covered by water values between 0.05 and $5 \cdot 10^9$ kg/km^2 (± one order of magnitude from our cutoff) is rather small compared to the overall "wet" area (Figure 3).

For a quantitative measure of the degree of correlation between IPV and wet MTZ, we determined the percentage of continental IPV locations positioned vertically above "wet" MTZ. We compared IPV and wet MTZ in this way for each 1 Myr time increment in the past, and averaged over the period 250–0 Ma.

3. Distribution of Water in the Mantle Transition Zone and Comparison to IPV

We compare predictive maps of MTZ water content with the changing locations of continental IPV through the past 250 Myr. We start by examining a reference scenario based on specific choices for t_{MTZ}, v_{sink}, and t_{IPV}. By adjusting these parameters, we develop alternative models for the timing of MTZ hydration, which we test against observed IPV patterns for t_{MTZ}, v_{sink}, and t_{IPV}.
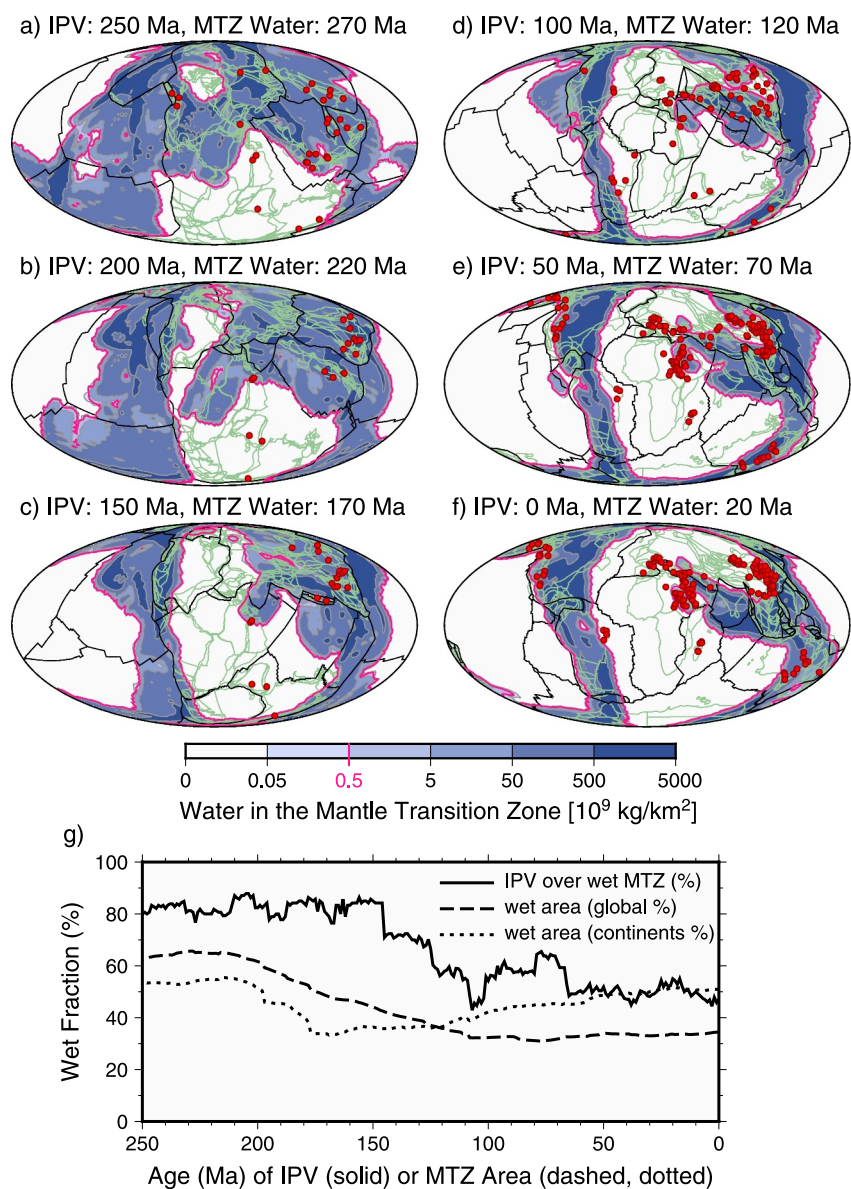
Figure 3. **Comparison of IPV locations to the MTZ water distribution for the reference scenario.** (a–f) Predictions of the water distribution in the mantle transition zone (colors) and locations of active continental intraplate volcanism (IPV, red points) for times between the present-day (a) and 250 Ma (f), with reconstructed outlines of continental blocks (green lines) and plate boundaries (black lines). The reference scenario shown here assumes that water has a residence time of $t_{MTZ} = 100$ Myr in the MTZ, a slab sinking velocity of $v_{sink} = 3$ cm/yr, and a $t_{IPV} = 20$ Myr delay before IPV eruption. (g) Percentage of IPV locations that lie above wet MTZ (defined as $\geq 0.5 \cdot 10^9$ kg/km^2, pink contour in a–f) for this reference scenario (solid line). Shown for comparison is the fraction of the reference grid area that is covered by hydrated (rather than dry) MTZ regions, both for the entire globe (dashed line) and for the portion of the grid identified as continental lithosphere (dotted line).

3.1. The Reference Scenario

For our reference scenario, we apply a sinking rate of $v_{sink} = 3$ cm/yr, an MTZ water residence time of $t_{MTZ} = 100$ Myr, and an IPV delay period of $t_{IPV} = 20$ Myr. This model predicts that at 20 Ma (Figure 3f) the hydrated portion of the MTZ extended across regions of the mantle transition zone beneath present-day South and North America, the western Pacific and eastern Asia, and beneath India and some of the Middle East. This hydrated MTZ reflects patterns of Cenozoic subduction, which is expected given that slabs sinking at 3 cm/yr will reach the MTZ after only 15–20 Myr. Because subduction migrates slowly, this same geographical pattern has

persisted since the Cretaceous (Figures 3d–3f), with about one third of the global MTZ and about half of the MTZ beneath continental areas being hydrated since 120 Ma (Figure 3g). Before the Cretaceous, the hydrated part of the global MTZ covered a larger area with weaker hydration (Figures 3a and 3b), reflecting slower regassing rates prior to ∼130 Ma (Karlsen et al., 2019) and faster trench migration rates prior to ∼250 Ma, perhaps resulting from ocean basin closure during supercontinent assembly (Young et al., 2019). More recently (since ∼150 Ma), trench retreat associated with Pangea breakup has moved continents increasingly above hydrated regions of the MTZ (Figures 3c–3f). This trend has resulted in an increase in the fractional area of continents sitting above the wet MTZ (Figure 3g). Nevertheless, wet areas represent a similar areal fraction of the global MTZ (43%) as for the sub-continental MTZ (45%) when averaged over the past 250 Myr.

We compare the 132 continental IPV samples for the present day (0 Ma) to the MTZ at 20 Ma, accounting for an assumed t_{IPV} = 20 Myr delay time before eruption (Figure 3f). We find that 47% of the 132 IPV samples overlie a wet MTZ (Figure 3g). Many of these "wet" IPV locations lie in eastern Asia and western North America (Figure 3f). Several points are located above MTZ that is only slightly hydrated, and some "dry" IPV locations are positioned near the western edges of hydrated MTZ, particularly during the past 50 Myr (Figures 3e and 3f) when ∼50% of IPV was underlain by wet MTZ (Figure 3g). The correspondence between IPV and wet MTZ was higher at 250 and 200 Ma (Figures 3a and 3b), with more than ∼80% of IPV underlain by MTZ that was wet 20 Myr prior (Figure 3g). This higher percentage likely results from a more geographically expansive wet MTZ (before ∼120 Ma globally or ∼180 Ma for continental regions, Figure 3g) from which our IPV catalog is sourced. Across 0–250 Ma, an average of 66.6% of continental IPV locations reconstruct above the MTZ that was wet 20 Myr before eruption. This fraction is greater than the 43%–45% area fraction represented by the wet MTZ.

3.2. MTZ Water Residence Time

By varying the MTZ residence time t_{MTZ}, we show that the volume of water in the MTZ increases with increased residence time, as expected (Figures 4a–4d). At 20 Ma (when MTZ hydration is compared to present-day IPV for t_{IPV} = 20 Myr), wet conditions extend across only ∼13% of the MTZ area for t_{MTZ} = 0 Myr (water sinks through the MTZ in less than 9 Myr at 3 cm/yr, Figure 4a), but across ∼74% if the MTZ if the residence time is unlimited (t_{MTZ} = ∞, Figure 4d). These trends are also evident for past times (e.g., at 100 and 200 Ma, Figure S4 in Supporting Information S1), where wet conditions tend to quickly "fill up" the MTZ for longer MTZ residence times. Because of this greater area-coverage of wet conditions, we find that more continental IPV locations lie above the hydrated MTZ for longer residence times (Figure 5a). As for the reference scenario (Figure 3a), the fraction of continental IPV underlain by wet MTZ is nearly always larger than the area fraction of the global wet MTZ (Figure 5a). This is also true for continental regions (Figure S5a in Supporting Information S1), although the fraction of wet MTZ area beneath continents tends to increase toward the wet IPV fraction after ∼120 Ma (Figure S5a in Supporting Information S1). This is because of the general movement of continents over the wet MTZ following Pangea breakup (Figure 3), which causes more of the wet MTZ area to be covered by continents at the expense of oceans (Figure S6a in Supporting Information S1). Thus, although all models show continental IPV locations preferentially occurring above wet areas of the global MTZ (Figure 5), this is less true when restricting this comparison to the continental portions of the wet MTZ since the Cretaceous (Figure S5 in Supporting Information S1).

3.3. Slab Sinking Rate

The slab sinking rate v_{sink} determines the time it takes for subducted water to reach the MTZ, and a slower sinking rate extends the time that water spends within the MTZ. However, varying the slab sinking rate between 1 and 9 cm/yr does not significantly change the predicted water distribution within the MTZ (Figures 4e–4h). Across the past 250 Myr (Figures 5b and Figure S5b in Supporting Information S1), a slow 1 cm/yr slab sinking rate results in a slightly higher fraction of IPV underlain by wet MTZ than for faster sinking rates. Again, the fraction of MTZ area that is wet is slightly higher for continental areas (Figure S5b in Supporting Information S1) than globally (Figure 5b), mostly because of recent continental motion above the wet MTZ (Figure S6b in Supporting Information S1).
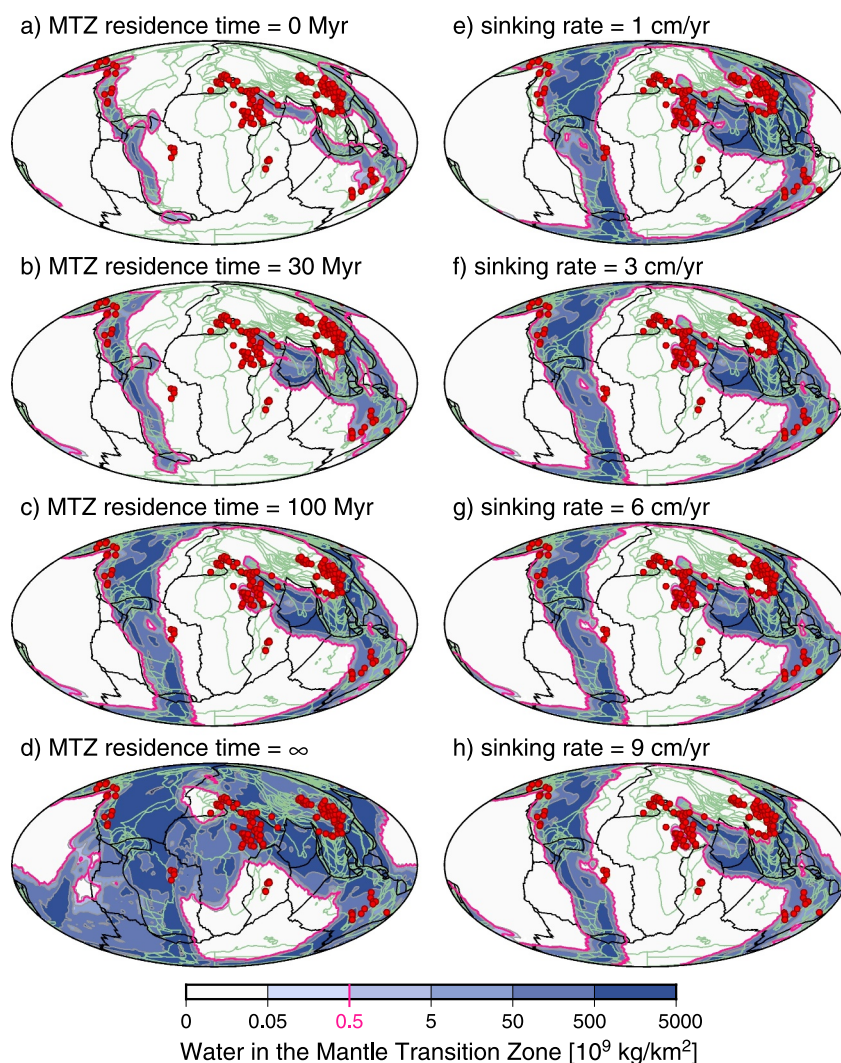
Figure 4. Effect of varying MTZ water residence time and slab sinking rates. Predictions of the water distribution in the mantle transition zone (MTZ) at 20 Ma for (a–d) varying MTZ residence time t_{MTZ} (assuming $v_{sink} = 3$ cm/yr and $t_{IPV} = 20$ Myr) and (e–h) varying slab sinking rate v_{sink} (assuming $t_{MTZ} = 100$ Myr and $t_{IPV} = 20$ Myr). Shown for all plots are continental blocks (green lines), plate boundaries (black lines) and active continental intraplate volcanism (IPV) locations (red dots) at 0 Ma. The pink contour outlines the wet MTZ (defined as $\geq 0.5 \cdot 10^9$ kg/km^2).

3.4. IPV Delay Period

Because the wet MTZ changes only gradually with time (e.g., Figure 3), the IPV delay period t_{IPV}, even one as long as 30 or 50 Myr, does not significantly affect the correlation between hydrated regions of the MTZ and IPV eruptions (Figures 5c and Figure S5c in Supporting Information S1). This parameter (t_{IPV}) also does not affect the area of the wet MTZ (dashed lines, Figure 5c) but effectively shifts the comparison toward younger ages (rightward in Figure 5c) because continental IPV eruption locations are compared to the MTZ at the (older) time before the delay. Because continental locations can change during this t_{IPV} period, the relevant wet MTZ area changes (mostly toward continents, Figure S6c in Supporting Information S1), slightly affecting area fractions (Figure S5c in Supporting Information S1).

4. Statistical Significance of Correlations

We use a statistical approach to determine whether the observed prevalence of continental IPV locations above hydrated regions of the MTZ (Figures 3g and 5, and Figure S5 in Supporting Information S1) can be considered significant. Specifically, we seek to test the null-hypothesis that the observed correlation can be explained as a
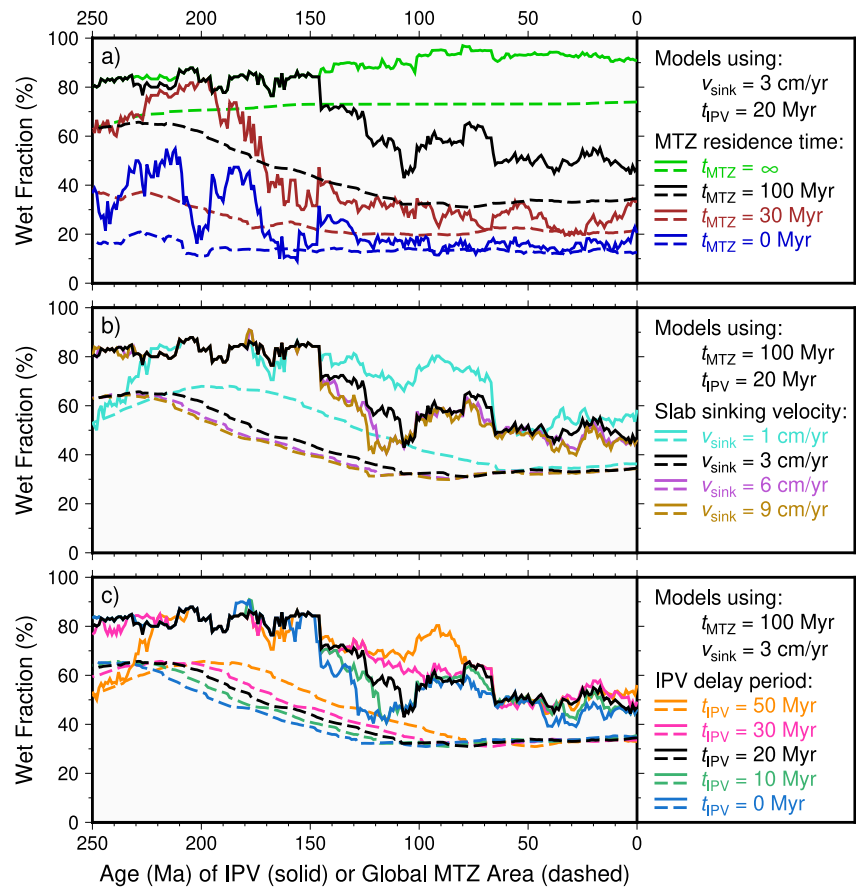
Figure 5. **The fraction of IPV locations and global MTZ areas sitting above hydrated MTZ for different scenarios.**
Shown are the fraction of continental intraplate volcanism (IPV) locations positioned above wet mantle transition zone
(MTZ, solid lines) and the representative fraction of global area covered by wet (rather than dry) MTZ regions (dashed lines).
(a) Varying MTZ residence times (t_{MTZ}) for scenarios with $v_{sink} = 3$ cm/yr and $t_{IPV} = 20$ Myr. (b) Varying slab sinking rates
(v_{sink}) for scenarios with $t_{MTZ} = 100$ Myr and $t_{IPV} = 20$ Myr. (c) Varying IPV delay periods (t_{IPV}) for scenarios with
$t_{MTZ} = 100$ Myr and $v_{sink} = 3$ cm/yr. The black lines reproduce the lines in Figure 3g, that is, the reference scenario.

chance occurrence. To achieve this, we compute the observed fit against a set of randomly perturbed trials and
conduct a one-tailed test. This allows us to determine the p-value, which is a measure of the likelihood of
obtaining a correlation as large or larger than the observed value by random chance, that is, the null-hypothesis. A
small p-value (typically $p < 0.05$) suggests that the null-hypothesis is unlikely, and can be rejected.

To develop a set of random comparisons from which to derive an empirical distribution, we randomly rotated each
simulated MTZ water grid (as constructed for a given set of model parameters, e.g., as shown in Figure 3 for the
reference scenario) about a randomly chosen rotation pole (see Text S4 in Supporting Information S1 for details).
To obtain a statistically significant sample, we randomly rotated each global MTZ water grid 10^4 times, applying
the same rotation for each time-step (within 0–250 Ma) of a given model. We then determined the fraction of
continental IPV locations (which remain unperturbed) occurring above wet MTZ for each randomly re-oriented
MTZ grid (see examples in Figure S7 in Supporting Information S1) and found the average over 250 million
years, as before. Applying this procedure to the 10^4 different random rotations, we constructed a distribution of
wet IPV fractions for these "randomized wet MTZ scenarios" (Figure 6). The p-value is given as the fraction of
this empirical distribution with a correlation between IPV and wet MTZ that is in excess of the observed value. If
less than 5% of the random re-orientations yield a higher wet IPV fraction ($p < 0.05$ in Figure 6), then we can
conclude that the observed correlation between IPV locations and the wet MTZ is not random. Note that the p-
value that we obtain using this method is independent of the number of volcanism samples and is valid even if IPV
sampling is incomplete (Conrad et al., 2011). This approach was applied to all scenarios of this study to determine
which correlations may be statistically significant.
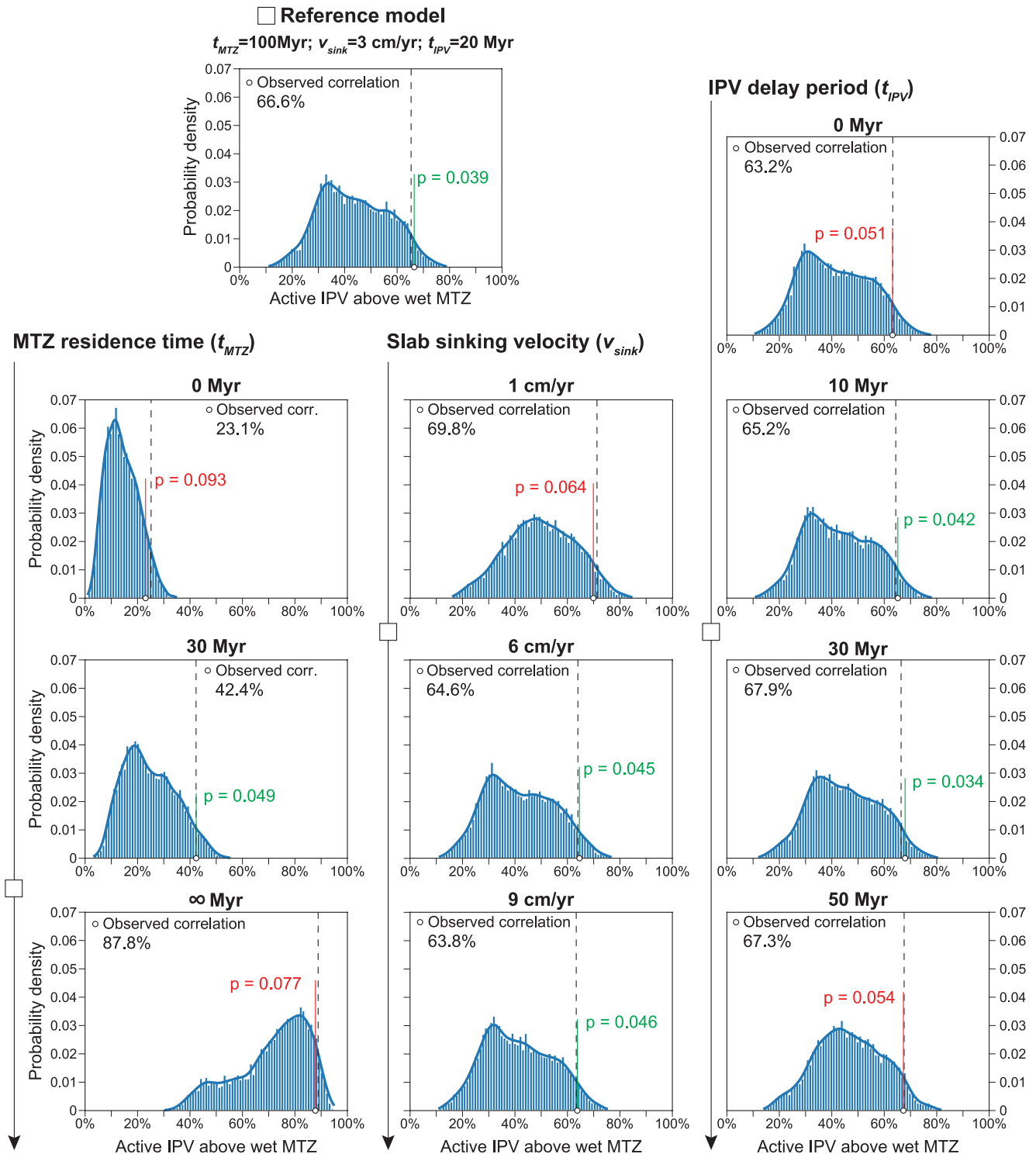
Figure 6. Distribution of correlations between continental IPV locations and randomly oriented wet MTZ for the various models of this study. The scenarios examined include the reference scenario (top left, marked with □), and variations to it involving the MTZ residence time (t_{MTZ}, left column), the slab sinking rate (v_{sink}, middle) and the IPV delay period (t_{IPV}, right). Here, the observed correlation (percentage of IPV locations underlain by wet MTZ) is drawn with a black dashed line (observed value given in black). The percentage of the distribution with a correlation larger than observed is given by the p-value, with $p < 0.05$ (shown by green labels) indicating that the observed correlation between continental IPV and wet MTZ is unlikely to result from random chance. In the remaining cases ($p > 0.05$, red labels), the null hypothesis cannot be rejected at the 95% confidence level.

For the reference scenario, 66.6% of continental IPV locations since 250 Ma are underlain by wet MTZ (Figure 5a and Section 3.1). Of the 10^4 re-oriented MTZ water grids, only 3.9% produced correlations greater than 66.6% (Figure 6, top). This corresponds to a p-value of 0.039, which satisfies $p < 0.05$ and means that we can reject the null hypothesis (that the observed correlation between IPV and wet MTZ is a chance occurrence) at the 95% confidence level. Applying the same procedure to the other models for the wet MTZ, in which we vary t_{MTZ}, v_{sink}, and t_{IPV} (Figure 6), we find that several other models exhibit correlations that are statistically significant at the 95% confidence level ($p \leq 0.05$). In particular, we find that changes to the reference scenario with t_{MTZ} of 30–100 Myr, v_{sink} of 3 cm/yr or more, and t_{IPV} between 10 and 30 Myr, can all produce correlations that are statistically significant at the 95% confidence level (Figure 6). These statistical tests suggest that there could be a meaningful link between the occurrence of continental IPV and hydrated regions of the MTZ, at least for the reference scenario and a range of models that are similar to it.

5. Discussion

We have mapped the spatial heterogeneity of water in the MTZ using tectonically reconstructed rates of water transport by subduction into the deep mantle during the past 400 Myr. We detected a statistically significant correlation (>95% confidence) between wet regions of the MTZ and continental locations of intraplate volcanism (42%–68% of IPV, Figure 6). This alignment of continental IPV locations with the wet MTZ occurs if MTZ water resides in the MTZ for a period (t_{MTZ}) between 30 and 100 Myr (Figure 6). Outside this range, shorter t_{MTZ} (e.g., 0 Myr) does not generate enough MTZ hydration to statistically explain continental IPV, while longer t_{MTZ} (e.g., case) hydrates so much of the MTZ that even randomly placed IPV locations are likely to sit above wet MTZ. This suggests that the temporary stagnation of slabs at the 660 km discontinuity, for periods of ~30 Myr or more, is crucial for MTZ hydration, and this hydration provides opportunities for continental IPV generation.

Different choices of slab sinking rate and IPV delay time do not significantly affect correlations between continental IPV and wet MTZ, except for their most extreme values. A relatively large p-value for $v_{sink} = 1$ cm/yr (Figure 6) indicates that a slow upper mantle sinking rate is not by itself sufficient to produce patterns of hydrated MTZ that are well correlated to IPV. Instead, it seems that stalling in the MTZ for ~30–100 Myr is necessary. We found that the most statistically significant IPV delay period (t_{IPV}) is 30 Myr (Figure 6). This timescale is roughly consistent with models (Long et al., 2019) that suggest a few 10's of Myr are needed for hydrous upwellings to form in the MTZ, ascend to the asthenosphere, melt, and erupt to the surface.

5.1. Implications for Intraplate Volcanism

Establishing that continental IPV patterns correlate with hydrous MTZ regions supports the widely recognized hypothesis that water is transported to the MTZ by subducting slabs (Bodnar et al., 2013; Kelbert et al., 2009; Magni et al., 2014; Thompson, 1992; van Keken et al., 2011), and consequently generates spatial and temporal mantle heterogeneity (Peslier et al., 2017). This also suggests that tectonic reconstruction models are a valuable tool for exploring and estimating this heterogeneity. Generally, the MTZ water distribution over the period investigated (0–250 Ma) reflects continuous hydration of particular regions with a long history of subduction. Many of these regions are overlain by IPV (e.g., Figure 3). Thus, the global association of continental IPV with the hydrated MTZ could potentially be explained by a variety of processes that generate upwelling in subduction-adjacent regions, such as "big mantle wedge" (BMW) return flow above stagnating slabs in the transition zone. Such upwelling flow has been linked to recent IPV in eastern Asia (e.g., Kameyama & Nishioka, 2012; Liang et al., 2022) and older IPV near ancient subduction systems (Cui et al., 2024), even without directly invoking a role for water. However, the proximity of subduction means that water likely permeates most BMW systems (Y. Wang & Xu, 2024), and this water has been shown to facilitate IPV (e.g., Yang & Faccenda, 2020), for example, by reducing melting temperatures and lowering viscosity. Thus, although other explanations are possible, our observed correlation between wet MTZ and continental IPV is likely best explained by the direct involvement of water in the generation of magmatism.

Upwelling from hydrated parts of the MTZ, and the subsequent generation of melting and IPV eruption may be a complicated process involving multiple geodynamic processes. For example, hydrous upwelling itself may require multiple subduction events to first saturate the MTZ and then to trigger upwelling flow of the hydrated mantle (Kuritani et al., 2011; Yang & Faccenda, 2020). Therefore, although the presence of water in the MTZ is likely to promote continental IPV, it must do so in conjunction with mantle processes that operate on MTZ

heterogeneity over time, including several that extract hydrated materials out of stagnant slabs and draw them upward (Kameyama & Nishioka, 2012; Kelbert et al., 2009; Long et al., 2019; Richard & Bercovici, 2009). Once hydrated rocks are in the asthenosphere, other processes such as shear-driven upwelling (e.g., Ballmer et al., 2015; Conrad et al., 2011), lithospheric deformation (e.g., Valentine & Hirano, 2010), small-scale convection (e.g., Ballmer et al., 2010; King & Ritsema, 2000), and return flow from slab-related downwelling (e.g., Kameyama & Nishioka, 2012; Liang et al., 2022) may be important to produce localized melting and eruption to the surface. Such processes may already be critical for generating IPV in drier areas and may amplify IPV in wet areas. Although we do not directly include these secondary processes within our models, we indirectly account for them when using large values of t_{MTZ} and t_{IPV} for which we obtain the largest correlations between continental IPV and wet MTZ.

5.2. Time-Dependent Hydration of the Mantle Transition Zone

Among the parameters we consider, the strongest control appears to be exerted by the MTZ water residence time (t_{MTZ}), which implies that slab stagnation is important for MTZ hydration. The extra time that stagnating slabs spend in the MTZ may provide opportunities for incorporation of subducted water into the hydrous reservoirs of the MTZ (e.g., Kuritani et al., 2011), which we have now associated with continental IPV at the surface. Storage of this water in the MTZ, even if temporary, removes water from the Earth's surface reservoirs, decreasing sea level (e.g., Karlsen et al., 2019). The presence of this water within the MTZ minerals of ringwoodite and wadsleyite may also be important for reducing MTZ viscosity toward observed values globally (Fei et al., 2017) and much reduced values locally (Park et al., 2023). This reduced viscosity may affect global mantle flow patterns (e.g., Karato, 2011), Earth's long-term thermal evolution (e.g., Crowley et al., 2011), and the processes that transport water laterally within the MTZ (Hebert & Montési, 2013).

Water loss from the MTZ may occur as mantle flow brings hydrated minerals across the upper (Andrault & Bolfan-Casanova, 2022) or lower (Schmandt et al., 2014) boundaries of the MTZ. The addition of water to the assemblage of nominally anhydrous minerals in these regions results in melting, and the melt likely percolates upward (Ohtani et al., 2018). Melt that forms above the MTZ eventually reaches the asthenosphere, and can be erupted as IPV (Andrault & Bolfan-Casanova, 2022). At some depths, this melt may be neutrally buoyant (Sakamaki, 2017) and interact with upper mantle flow (Leahy & Bercovici, 2010), potentially complicating spatial and temporal correlations with IPV. Melt forming below the MTZ may also percolate upward, re-hydrating the MTZ (Schmandt et al., 2014), but some water likely remains stored within lower mantle bridgmanite, and continues downward (Mohn et al., 2025; Walter, 2021). Our results suggest that these processes overall lead to an average longevity of water in the MTZ of order 30–100 Myr, with much uncertainty.

Seismic detection of basaltic heterogeneities, which are brought downward by slabs and linked to MTZ water storage (Ohtani, 2019), may provide an independent constraint on MTZ hydration patterns and the MTZ residence time (t_{MTZ}). Tauzin et al. (2022) detected a correlation between basaltic heterogeneities and the past ~100 Myr of subduction (Tauzin et al., 2022), as we have found for water (e.g., Figure 3). This suggests that the lifetime of hydrous and basaltic heterogeneities in the MTZ may be comparable, and supports our constraints on t_{MTZ}. Some mantle flow models that track basaltic heterogeneities suggest much longer timescales (e.g., Yan et al., 2020) because basaltic heterogeneities can become gravitationally trapped within the MTZ in regions away from subduction zones (Tauzin et al., 2022). It is not known if elevated MTZ hydration may be associated with such trapped basaltic heterogeneities, but we do not find a statistically significant correlation of continental IPV with MTZ hydration enduring significantly longer than 100 Myr (Figure 6).

Our models suggest that ever since Pangea breakup, the area of wet MTZ beneath continents has been increasing (Figure S6 in Supporting Information S1). This increase is associated with the movement of continents (particularly the America and Australia, Figure 3) above the already-hydrated parts of the MTZ. It is difficult to determine whether this greater hydration beneath continents could have led to more continental IPV because the observed increase in IPV locations during this period (Figure S3c in Supporting Information S1) may simply result from sampling bias. Furthermore, we observe that a greater fraction of continental IPV locations lie above the hydrated MTZ (solid lines, Figure 5) in the first half of our reconstruction (~125–250 Ma), not the more recent half. This is the opposite of what we might expect, given the smaller hydrated areas beneath continents (Figure S6 in Supporting Information S1) and greater uncertainties for both the plate reconstruction and the IPV database moving backward into the past. However, large regassing rates early in the tectonic reconstruction (before
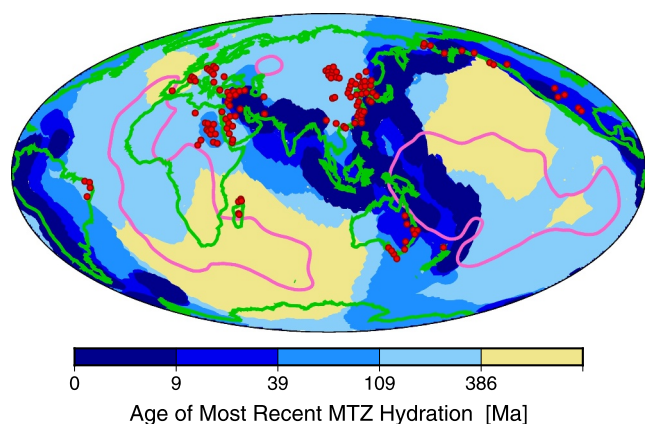
Figure 7. **Map of the age of the most recent MTZ hydration** (colors) as compared to current continental intraplate volcanism locations (red dots), current continental outlines (green lines), and LLSVP locations at the base of the mantle (pink lines). Here we assume a slab sinking rate of 3 cm/yr, and plot colors based on the ages of interaction of slabs with the MTZ for the four different choices of t_{MTZ} that we examined. We note that three major areas of the MTZ (regions with yellow colors, near western Europe, southern Africa and the northern Pacific) have not interacted with hydrated slabs in the past 400 Myr.

320 Ma, Figure S1e in Supporting Information S1) and rapid trench migration (Young et al., 2019) may have hydrated significant parts of the MTZ during the period ~400–200 Ma. The storage of this water in the MTZ for periods of up to 100 Myr (large MTZ residence times) may have induced IPV across a wide region during the first part of our analysis (~250–150 Ma). Alternatively, if sampling bias explains the smaller number of continental IPV samples for older times (Figure S3c in Supporting Information S1), then this bias may involve preferential sampling of eruptions that are larger in magnitude (greater eruptive volume). Such events may result from melting of the hydrous upper mantle, which should produce greater melt volumes. By contrast, the database of recent continental IPV may over-represent small-scale events that are less likely to be related to wet MTZ.

5.3. Dry Regions of the Mantle Transition Zone

The water mapped in this study is transported to the MTZ by subduction. Therefore, areas that have remained far from subduction zones throughout the considered period may be relatively dry (Figure 7), unless ancient water has remained stable for longer periods (>400 Myr) or water has been transported into these regions by other means. This suggests that the MTZ beneath the Indian Ocean, Southeast Africa, the South Atlantic Ocean, large parts of the North Pacific Ocean, and a modest area below western Europe have remained dry for the past 400 Myr, and could be dry today. We note that there is relatively little IPV above the "dry" areas, although many of these regions are covered by oceanic lithosphere, where we have not considered IPV. These "dry" areas away from subduction zones roughly correspond to areas of persistent and stable broad-scale upwelling in the mantle (Conrad et al., 2013), which represents a return-flow from subduction downwelling occurring around these areas (Shephard et al., 2017). Intraplate volcanism has been identified within these regions away from subduction, but it has been mostly associated with mantle plumes (e.g., Hawaii) driven upward from the deepest mantle by their thermal buoyancy. Plume-induced intraplate volcanism has been associated with the edges of the Large Low Shear Velocity Provinces (LLSVPs) at the base of the mantle, which form away from subduction zones (Torsvik et al., 2016). Some of the continental IPV identified within the "dry" areas of the MTZ (Figure 7) may thus be associated with plumes rising from the deep mantle.

Because the presence of water tends to reduce the viscosity of the MTZ (Fei et al., 2017), these dry regions should have a larger viscosity than the wetter areas that surround them. If so, then mantle deformation may preferentially occur in the wetter areas, affecting upper mantle flow patterns (Ramirez et al., 2023). Indeed, subduction-related deformation has tended to occur away from these potentially dry areas above the LLSVPs (Shephard et al., 2017), preventing hydration of these parts of the MTZ (Figure 7) and perhaps stabilizing large-scale mantle flow patterns (Conrad et al., 2013). A dry MTZ may also exert an important influence on rates of glacial isostatic adjustment (GIA), which includes the solid Earth's viscous response to episodes of deglaciation. Indeed, one of the dry regions in our models is predicted to extend beneath East Antarctica (Figure 7). Here, elevated upper mantle viscosities have been shown to slow rates of uplift in response to past (and future) deglaciation, with important implications for sea level change (Gomez et al., 2024).

5.4. Future Outlook

Uncertainties in the generated MTZ water grids are partly linked to and controlled by the underlying plate tectonic model (Karlsen et al., 2020, 2021; Matthews et al., 2016; Torsvik et al., 2019), which becomes increasingly poorly constrained for older time periods. We assume vertical subduction, which is reasonable for mapping subducted slabs (Domeier et al., 2016), but does not account for lateral deflections or slab stagnation that may affect the MTZ water content. Thus, we have had to introduce additional parameterizations, such as the threshold for wet MTZ and the number of nearest neighbors used to spread the water laterally. These choices are poorly constrained and affect the MTZ water distribution and its link to continental IPV. We argue that the statistical approach used here (Section 4) allows us to overcome this uncertainty by looking for overall correlations, even weak ones, based on "best guess" choices for some of these unknown parameters. However, more tightly linking subduction history, MTZ hydration, and continental IPV in certain regions, for example, using regional observations and

modeling, may provide better constraints on the processes that extract water from the slab and move it upward or laterally within the MTZ (e.g., Long et al., 2019; Richard & Bercovici, 2009; Yang & Faccenda, 2020).

We have shown that one of the most important parameters is the MTZ residence time, which is related to slab stagnation. However, not all slabs behave the same way; some may stagnate for different amounts of time in the MTZ while others subduct directly through it. Therefore, our assumption of using one constant value of MTZ residence time per model is a significant simplification. More detailed maps of wet and dry regions in the mantle transition zone (Figure 7) could be constructed by considering these different behaviors for each slab. It could be possible to infer slab topology from tomographic models for recent times. For past times, one could use the location and ages of IPV to speculate on the temporal and spatial variations of the MTZ hydration state back in time.

We chose a low value of $0.5 \cdot 10^9$ kg/km^2 for the threshold between wet and dry MTZ. A low threshold is reasonable as even a tiny amount of water can generate melt production if the mantle conditions are close to the solidus (Hirschmann, 2006; Katz et al., 2003), although buoyant hydrous upwelling may require significant hydration (e.g., Long et al., 2019; Richard & Bercovici, 2009; Yang & Faccenda, 2020). Eventually, it could be useful to investigate correlations between the degree of MTZ hydration and the volumes of IPV, although IPV volumes can be difficult to estimate, especially given different uncertainties for intrusive and extrusive components (e.g., Heyn et al., 2024). Overall, an improved understanding of the mechanistic links between MTZ water and hydrous upwelling and melting could help us better link MTZ heterogeneity with non-hotspot IPV.

6. Conclusions

Our study suggests that the mantle transition zone (MTZ, 410–660 km) is likely to be heterogeneously hydrated, with wetter regions beneath areas with a long history of subduction, and regions away from subduction remaining dry (Figure 7). To show this, we created maps of the spatial and temporal heterogeneity of water storage in the mantle transition zone (e.g., Figure 3) based on tectonic reconstructions for the last 400 Ma and the assumption that subduction transports water downward into the MTZ. Using these maps, we discovered a positive correlation between wet regions of the MTZ and locations of continental intraplate volcanism (IPV) at the surface (Figure 5) and demonstrated that this correlation is statistically significant (Figure 6). In particular, we showed that water must reside in the MTZ for long periods (timescales of 30–100 Myr) in order for the hydrous regions of the MTZ to be positively correlated with IPV in a statistically significant way (>95% confidence that the association is not random). This period of slab stagnation facilitates slab dehydration and water accumulation in the surrounding MTZ rocks. We also found that a time delay of 10–30 Myr before IPV eruption tends to produce better correlations. The long delay between the subduction of water and the eventual triggering of IPV much later suggests that significant time and perhaps multiple subduction events are required to hydrate the MTZ, mobilize the hydrated mantle to generate melt, and transport this melt upwards for eruption at the surface.

The MTZ water distribution, as characterized by our predictive maps (Figures 3 and 4), is mostly dictated by tectonic patterns of subduction at the surface, including the plate convergence rate, trench migration rate, and subducting plate age for subduction zones around the world (Karlsen et al., 2019). We find that the area fraction of wet MTZ was likely greater in the past (>150 Ma) because of a more extensive subduction network that migrated more quickly (Young et al., 2019). However, the area of wet MTZ beneath continents has been growing since the breakup of Pangea (Figure S6 in Supporting Information S1) due to continental movements (particularly of the Americas and Australia) above wet portions of the MTZ (Figure 3). The extent of hydration also depends critically on the residence time of water in the MTZ, as controlled by slab stagnation (Komabayashi & Omori, 2006; Kuritani et al., 2011) and possible MTZ rehydration (Schmandt et al., 2014) as water is released from dehydrating slabs in the uppermost lower mantle (Walter, 2021). Also important are processes that generate upwelling and upward water transport from the hydrous regions of the MTZ (e.g., Kuritani et al., 2019; Richard & Bercovici, 2009; X.-C. Wang et al., 2015; Yang & Faccenda, 2020), leading to melting beneath the lithosphere (e.g., Long et al., 2019; Motoki & Ballmer, 2015) and eruption at the surface.

Our study suggests that water stored within the MTZ exerts a controlling influence on global patterns of intraplate volcanism. This water is brought to the MTZ by ancient subduction and stays there on timescales of 30–100 Myr. This link between MTZ water storage and continental IPV provides a unified explanation for present-day volcanism in eastern Asia, western North America, and eastern Australia, and explains the distribution of continental intraplate volcanism over the past ~200 Myr. Beyond these important implications for IPV, a

heterogeneously hydrated MTZ should also be viscously heterogeneous (Fei et al., 2017). This is important because MTZ viscosity controls rates of upper mantle flow (Ramirez et al., 2023), planetary thermal evolution (Crowley et al., 2011), and even recent deglaciation-induced solid earth uplift (Gomez et al., 2024). Thus, new comparisons between geophysical, geologic, and tectonic constraints on the hydration state of the MTZ, exemplified by our study, can help us to understand a variety of important geodynamic processes.

Data Availability Statement

The intraplate volcanism database is taken from the GEOROC (Geochemistry of Rocks of the Oceans and Continents, https://georoc.eu/) database, with data available from Lehnert et al. (2000). To create maps of the hydrous regions of the mantle transition zone, we utilized the GPlates software (Müller et al., 2018) (which can be accessed at https://www.gplates.org), data from the global plate tectonic model of Matthews et al. (2016) with corrections for the Pacific from Torsvik et al. (2019), and seafloor ages from Karlsen et al. (2021).

References

Aivazpourporgou, S., Thiel, S., Hayman, P. C., Moresi, L. N., & Heinson, G. (2015). Decompression melting driving intraplate volcanism in Australia: Evidence from magnetotelluric sounding. *Geophysical Research Letters*, *42*(2), 2014GL060088. https://doi.org/10.1002/2014GL060088

Andrault, D., & Bolfan-Casanova, N. (2022). Mantle rain toward the Earth's surface: A model for the internal cycle of water. *Physics of the Earth and Planetary Interiors*, *322*, 106815. https://doi.org/10.1016/j.pepi.2021.106815

Ballmer, M. D., Conrad, C. P., Smith, E. I., & Johnsen, R. (2015). Intraplate volcanism at the edges of the Colorado Plateau sustained by a combination of triggered edge-driven convection and shear-driven upwelling. *Geochemistry, Geophysics, Geosystems*, *16*(2), 366–379. https://doi.org/10.1002/2014GC005641

Ballmer, M. D., Ito, G., van Hunen, J., & Tackley, P. J. (2010). Small-scale sublithospheric convection reconciles geochemistry and geochronology of "Superplume" volcanism in the western and south Pacific. *Earth and Planetary Science Letters*, *290*(1–2), 224–232. https://doi.org/10.1016/j.epsl.2009.12.025

Bercovici, D., & Karato, S.-I. (2003). Whole-mantle convection and the transition-zone water filter. *Nature*, *425*(6953), 39–44. https://doi.org/10.1038/nature01918

Bodnar, R. J., Azbej, T., Becker, S. P., Cannatelli, C., Fall, A., & Severs, M. J. (2013). Whole Earth geohydrologic cycle, from the clouds to the core: The distribution of water in the dynamic Earth system. *Geological Society of America Special Paper*, *500*(13), 431–461. https://doi.org/10.1130/2013.2500

Butterworth, N. P., Talsma, A. S., Müller, R. D., Seton, M., Bunge, H. P., Schuberth, B. S. A., et al. (2014). Geological, tomographic, kinematic and geodynamic constraints on the dynamics of sinking slabs. *Journal of Geodynamics*, *73*, 1–13. https://doi.org/10.1016/j.jog.2013.10.006

Chang, S.-J., & Ferreira, A. M. G. (2019). Inference on water content in the mantle transition zone near subducted slabs from anisotropy tomography. *Geochemistry, Geophysics, Geosystems*, *20*(2), 1189–1201. https://doi.org/10.1029/2018gc008090

Conrad, C. P., Bianco, T. A., Smith, E. I., & Wessel, P. (2011). Patterns of intraplate volcanism controlled by asthenospheric shear. *Nature Geoscience*, *4*(5), 317–321. https://doi.org/10.1038/ngeo1111

Conrad, C. P., Selway, K., Hirschmann, M. M., Ballmer, M. D., & Wessel, P. (2017). Constraints on volumes and patterns of asthenospheric melt from the space-time distribution of seamounts. *Geophysical Research Letters*, *44*(14), 7203–7210. https://doi.org/10.1002/2017GL074098

Conrad, C. P., Steinberger, B., & Torsvik, T. H. (2013). Stability of active mantle upwelling revealed by net characteristics of plate tectonics. *Nature*, *498*(7455), 479–482. https://doi.org/10.1038/nature12203

Courtillot, V., Davaille, A., Besse, J., & Stock, J. (2003). Three distinct types of hotspots in the Earth's mantle. *Earth and Planetary Science Letters*, *205*(3–4), 295–308. https://doi.org/10.1016/S0012-821X(02)01048-8

Crowley, J. W., Gérault, M., & O'Connell, R. J. (2011). On the relative influence of heat and water transport on planetary dynamics. *Earth and Planetary Science Letters*, *310*(3–4), 380–388. https://doi.org/10.1016/j.epsl.2011.08.035

Cui, X., Cawood, P. A., Sun, M., & Zhao, G. (2024). Recognizing big mantle wedges in deep time: Constraints from the Western Mongolia Collage in Central Asia. *Geology*, *52*(5), 341–346. https://doi.org/10.1130/g51841.1

Demouchy, S., & Bolfan-Casanova, N. (2016). Distribution and transport of hydrogen in the lithospheric mantle: A review. *Lithos*, *240–243*, 402–425. https://doi.org/10.1016/j.lithos.2015.11.012

Domeier, M., Doubrovine, P. V., Torsvik, T. H., Spakman, W., & Bull, A. L. (2016). Global correlation of lower mantle structure and past subduction. *Geophysical Research Letters*, *43*(10), 4945–4953. https://doi.org/10.1002/2016GL068827

Fei, H., Yamazaki, D., Sakurai, M., Miyajima, N., Ohfuji, H., Katsura, T., & Yamamoto, T. (2017). A nearly water-saturated mantle transition zone inferred from mineral viscosity. *Science Advances*, *3*(6). https://doi.org/10.1126/sciadv.1603024

Gevorgian, J., Sandwell, D. T., Yu, Y., Kim, S.-S., & Wessel, P. (2023). Global distribution and morphology of small seamounts. *Earth and Space Science*, *10*(4), e2022EA002331. https://doi.org/10.1029/2022EA002331

Goes, S., Agrusta, R., van Hunen, J., & Garel, F. (2017). Subduction-transition zone interaction: A review. *Geosphere*, *13*(7), 644–664. https://doi.org/10.1130/GES01476.1

Goes, S., Capitanio, F. A., Morra, G., Seton, M., & Giardini, D. (2011). Signatures of downgoing plate-buoyancy driven subduction in Cenozoic plate motions. *Physics of the Earth and Planetary Interiors*, *184*(1), 1–13. https://doi.org/10.1016/j.pepi.2010.10.007

Gomez, N., Yousefi, M., Pollard, D., DeConto, R. M., Sadai, S., Lloyd, A., et al. (2024). The influence of realistic 3D mantle viscosity on Antarctica's contribution to future global sea levels. *Science Advances*, *10*(31), eadn1470. https://doi.org/10.1126/sciadv.adn1470

Hebert, L. B., & Montési, L. G. J. (2013). Hydration adjacent to a deeply subducting slab: The roles of nominally anhydrous minerals and migrating fluids. *Journal of Geophysical Research: Solid Earth*, *118*(11), 2013JB010497. https://doi.org/10.1002/2013JB010497

Hernlund, J. W., Stevenson, D. J., & Tackley, P. J. (2008). Buoyant melting instabilities beneath extending lithosphere: 2. Linear analysis. *Journal of Geophysical Research*, *113*(B4). https://doi.org/10.1029/2006JB004863

Heyn, B. H., & Conrad, C. P. (2022). On the relation between basal erosion of the lithosphere and surface heat flux for continental plume tracks. *Geophysical Research Letters*, *49*(7), e2022GL098003. https://doi.org/10.1029/2022GL098003

Heyn, B. H., Shephard, G. E., & Conrad, C. P. (2024). Prolonged multi-phase magmatism due to plume-lithosphere interaction as applied to the High Arctic Large Igneous Province. *Geochemistry, Geophysics, Geosystems*, *25*(6), e2023GC011380. https://doi.org/10.1029/2023GC011380

Hier-Majumder, S., & Tauzin, B. (2017). Pervasive upper mantle melting beneath the western US. *Earth and Planetary Science Letters*, *463*, 25–35. https://doi.org/10.1016/j.epsl.2016.12.041

Hirschmann, M. M. (2006). Water, melting, and the deep earth H_2O cycle. *Annual Review of Earth and Planetary Sciences*, *34*(1), 629–653. https://doi.org/10.1146/annurev.earth.34.031405.125211

Houser, C. (2016). Global seismic data reveal little water in the mantle transition zone. *Earth and Planetary Science Letters*, *448*, 94–101. https://doi.org/10.1016/j.epsl.2016.04.018

Huang, X., Xu, Y., & Karato, S.-I. (2005). Water content in the transition zone from electrical conductivity of wadsleyite and ringwoodite. *Nature*, *434*(7034), 746–749. https://doi.org/10.1038/nature03426

Inoue, T., Tanimoto, Y., Irifune, T., Suzuki, T., Fukui, H., & Ohtaka, O. (2004). Thermal expansion of wadsleyite, ringwoodite, hydrous wadsleyite and hydrous ringwoodite. *Physics of the Earth and Planetary Interiors*, *143–144*, 279–290. https://doi.org/10.1016/j.pepi.2003.07.021

Kameyama, M., & Nishioka, R. (2012). Generation of ascending flows in the Big Mantle Wedge (BMW) beneath northeast Asia induced by retreat and stagnation of subducted slab. *Geophysical Research Letters*, *39*(10). https://doi.org/10.1029/2012GL051678

Karato, S.-I. (2011). Water distribution across the mantle transition zone and its implications for global material circulation. *Earth and Planetary Science Letters*, *301*(3–4), 413–423. https://doi.org/10.1016/j.epsl.2010.11.038

Karato, S.-I., Karki, B., & Park, J. (2020). Deep mantle melting, global water circulation and its implications for the stability of the ocean mass. *Progress in Earth and Planetary Science*, *7*(1), 76. https://doi.org/10.1186/s40645-020-00379-3

Karlsen, K. S., Conrad, C. P., Domeier, M., & Trønnes, R. G. (2021). Spatiotemporal variations in surface heat loss imply a heterogeneous mantle cooling history. *Geophysical Research Letters*, *48*(6), e2020GL092119. https://doi.org/10.1029/2020GL092119

Karlsen, K. S., Conrad, C. P., & Magni, V. (2019). Deep water cycling and sea level change since the breakup of Pangea. *Geochemistry, Geophysics, Geosystems*, *20*(6), 2919–2935. https://doi.org/10.1029/2019GC008232

Karlsen, K. S., Domeier, M., Gaina, C., & Conrad, C. P. (2020). A tracer-based algorithm for automatic generation of seafloor age grids from plate tectonic reconstructions. *Computers and Geosciences*, *140*, 104508. https://doi.org/10.1016/j.cageo.2020.104508

Katz, R. F., Spiegelman, M., & Langmuir, C. H. (2003). A new parameterization of hydrous mantle melting. *Geochemistry, Geophysics, Geosystems*, *4*(9). https://doi.org/10.1029/2002GC000433

Kelbert, A., Schultz, A., & Egbert, G. (2009). Global electromagnetic induction constraints on transition-zone water content variations. *Nature*, *460*(7258), 1003–1006. https://doi.org/10.1038/nature08257

King, S. D., & Ritsema, J. (2000). African hot spot volcanism: Small-scale convection in the upper mantle beneath cratons. *Science*, *290*(5494), 1137–1140. https://doi.org/10.1126/science.290.5494.1137

Komabayashi, T., & Omori, S. (2006). Internally consistent thermodynamic data set for dense hydrous magnesium silicates up to 35 GPa, 1600°C: Implications for water circulation in the Earth's deep mantle. *Physics of the Earth and Planetary Interiors*, *156*(1), 89–107. https://doi.org/10.1016/j.pepi.2006.02.002

Kuritani, T., Ohtani, E., & Kimura, J.-I. (2011). Intensive hydration of the mantle transition zone beneath China caused by ancient slab stagnation. *Nature Geoscience*, *4*(10), 713–716. https://doi.org/10.1038/ngeo1250

Kuritani, T., Xia, Q.-K., Kimura, J.-I., Liu, J., Shimizu, K., Ushikubo, T., et al. (2019). Buoyant hydrous mantle plume from the mantle transition zone. *Scientific Reports*, *9*(1), 6549. https://doi.org/10.1038/s41598-019-43103-y

Leahy, G. M., & Bercovici, D. (2010). Reactive infiltration of hydrous melt above the mantle transition zone. *Journal of Geophysical Research*, *115*(B8). https://doi.org/10.1029/2009JB006757

Lehnert, K., Su, Y., Langmuir, C. H., Sarbas, B., & Nohl, U. (2000). A global geochemical database structure for rocks. *Geochemistry, Geophysics, Geosystems*, *1*(5). https://doi.org/10.1029/1999GC000026

Liang, X., Zhao, D., Xu, Y.-G., & Hua, Y. (2022). Anisotropic tomography and dynamics of the big mantle wedge. *Geophysical Research Letters*, *49*(5), e2021GL097550. https://doi.org/10.1029/2021GL097550

Long, X., Ballmer, M. D., Córdoba, A. M.-C., & Li, C.-F. (2019). Mantle melting and intraplate volcanism due to self-buoyant hydrous upwellings from the stagnant slab that are conveyed by small-scale convection. *Geochemistry, Geophysics, Geosystems*, *20*(11), 4972–4997. https://doi.org/10.1029/2019gc008591

Magni, V., Bouilhol, P., & van Hunen, J. (2014). Deep water recycling through time. *Geochemistry, Geophysics, Geosystems*, *15*(11), 4203–4216. https://doi.org/10.1002/2014GC005525

Matthews, K. J., Maloney, K. T., Zahirovic, S., Williams, S. E., Seton, M., & Müller, R. D. (2016). Global plate boundary evolution and kinematics since the late Paleozoic. *Global and Planetary Change*, *146*, 226–250. https://doi.org/10.1016/j.gloplacha.2016.10.002

Meier, U., Trampert, J., & Curtis, A. (2009). Global variations of temperature and water content in the mantle transition zone from higher mode surface waves. *Earth and Planetary Science Letters*, *282*(1), 91–101. https://doi.org/10.1016/j.epsl.2009.03.004

Mohn, C. E., Caracas, R., & Conrad, C. P. (2025). Lower mantle water distribution from ab initio proton diffusivity in bridgmanite. *Earth and Planetary Science Letters*, *649*, 119095. https://doi.org/10.1016/j.epsl.2024.119095

Motoki, M. H., & Ballmer, M. D. (2015). Intraplate volcanism due to convective instability of stagnant slabs in the mantle transition zone. *Geochemistry, Geophysics, Geosystems*, *16*(2), 538–551. https://doi.org/10.1002/2014GC005608

Müller, R. D., Cannon, J., Qin, X., Watson, R. J., Gurnis, M., Williams, S., et al. (2018). GPlates: Building a virtual Earth through deep time. *Geochemistry, Geophysics, Geosystems*, *19*(7), 2243–2261. https://doi.org/10.1029/2018GC007584

Nestola, F., & Smyth, J. R. (2016). Diamonds and water in the deep Earth: A new scenario. *International Geology Review*, *58*(3), 263–276. https://doi.org/10.1080/00206814.2015.1056758

Ohtani, E. (2019). The role of water in Earth's mantle. *National Science Review*, *7*(1), 224–232. https://doi.org/10.1093/nsr/nwz071

Ohtani, E., Yuan, L., Ohira, I., Shatskiy, A., & Litasov, K. (2018). Fate of water transported into the deep mantle by slab subduction. *Journal of Asian Earth Sciences*, *167*, 2–10. https://doi.org/10.1016/j.jseaes.2018.04.024

Panero, W. R. (2010). First principles determination of the structure and elasticity of hydrous ringwoodite. *Journal of Geophysical Research*, *115*(B3). https://doi.org/10.1029/2008JB006282

Park, S., Avouac, J.-P., Zhan, Z., & Gualandi, A. (2023). Weak upper-mantle base revealed by postseismic deformation of a deep earthquake. *Nature*, *615*(7952), 455–460. https://doi.org/10.1038/s41586-022-05689-8

Pearson, D. G., Brenker, F. E., Nestola, F., McNeill, J., Nasdala, L., Hutchison, M. T., et al. (2014). Hydrous mantle transition zone indicated by ringwoodite included within diamond. *Nature*, *507*(7491), 221–224. https://doi.org/10.1038/nature13080

Peslier, A. H., Schönbächler, M., Busemann, H., & Karato, S.-I. (2017). Water in the Earth's interior: Distribution and origin. *Space Science Reviews*, *212*(1), 743–810. https://doi.org/10.1007/s11214-017-0387-z

Ramirez, F. D. C., Conrad, C. P., & Selway, K. (2023). Grain size reduction by plug flow in the wet oceanic upper mantle explains the asthenosphere's low seismic Q zone. *Earth and Planetary Science Letters*, *616*, 118232. https://doi.org/10.1016/j.epsl.2023.118232

Ramirez, F. D. C., Selway, K., Conrad, C. P., & Lithgow-Bertelloni, C. (2022). Constraining upper mantle viscosity using temperature and water content inferred from seismic and magnetotelluric data. *Journal of Geophysical Research: Solid Earth*, *127*(8), e2021JB023824. https://doi.org/10.1029/2021JB023824

Richard, G. C., & Bercovici, D. (2009). Water-induced convection in the Earth's mantle transition zone. *Journal of Geophysical Research*, *114*(B1). https://doi.org/10.1029/2008JB005734

Rüpke, L. H., Morgan, J. P., Hort, M., & Connolly, J. A. D. (2004). Serpentine and the subduction zone water cycle. *Earth and Planetary Science Letters*, *223*(1–2), 17–34. https://doi.org/10.1016/j.epsl.2004.04.018

Sakamaki, T. (2017). Density of hydrous magma. *Chemical Geology*, *475*, 135–139. https://doi.org/10.1016/j.chemgeo.2017.11.012

Schmandt, B., Jacobsen, S. D., Becker, T. W., Liu, Z., & Dueker, K. G. (2014). Dehydration melting at the top of the lower mantle. *Science*, *344*(6189), 1265–1268. https://doi.org/10.1126/science.1253358

Schulze, K., Marquardt, H., Kawazoe, T., Boffa Ballaran, T., McCammon, C., Koch-Müller, M., et al. (2018). Seismically invisible water in Earth's transition zone? *Earth and Planetary Science Letters*, *498*, 9–16. https://doi.org/10.1016/j.epsl.2018.06.021

Shephard, G. E., Matthews, K. J., Hosseini, K., & Domeier, M. (2017). On the consistency of seismically imaged lower mantle slabs. *Scientific Reports*, *7*(1), 10976. https://doi.org/10.1038/s41598-017-11039-w

Shirey, S. B., Wagner, L. S., Walter, M. J., Pearson, D. G., & van Keken, P. E. (2021). Slab transport of fluids to deep focus earthquake depths—Thermal modeling constraints and evidence from diamonds. *AGU Advances*, *2*(2), e2020AV000304. https://doi.org/10.1029/2020AV000304

Suetsugu, D., Inoue, T., Yamada, A., Zhao, D., & Obayashi, M. (2006). Towards mapping the three-dimensional distribution of water in the transition zone from P-velocity tomography and 660-km discontinuity depths. In *Earth's deep water cycle* (pp. 237–249). https://doi.org/10.1029/168GM18

Syracuse, E. M., van Keken, P. E., & Abers, G. A. (2010). The global range of subduction zone thermal models. *Physics of the Earth and Planetary Interiors*, *183*(1–2), 73–90. https://doi.org/10.1016/j.pepi.2010.02.004

Tauzin, B., Waszek, L., Ballmer, M. D., Afonso, J. C., & Bodin, T. (2022). Basaltic reservoirs in the Earth's mantle transition zone. *Proceedings of the National Academy of Sciences of the United States of America*, *119*(48), e2209399119. https://doi.org/10.1073/pnas.2209399119

Thompson, A. B. (1992). Water in the Earth's upper mantle. *Nature*, *358*(6384), 295–302. https://doi.org/10.1038/358295a0

Torsvik, T. H., Steinberger, B., Ashwal, L. D., Doubrovine, P. V., & Trønnes, R. G. (2016). Earth evolution and dynamics—A tribute to Kevin Burke. *Canadian Journal of Earth Sciences*, *53*(11), 1073–1087. https://doi.org/10.1139/cjes-2015-0228

Torsvik, T. H., Steinberger, B., Shephard, G. E., Doubrovine, P. V., Gaina, C., Domeier, M., et al. (2019). Pacific-panthalassic reconstructions: Overview, errata and the way forward. *Geochemistry, Geophysics, Geosystems*, *20*(7), 3659–3689. https://doi.org/10.1029/2019gc008402

Valentine, G. A., & Hirano, N. (2010). Mechanisms of low-flux intraplate volcanic fields—Basin and range (North America) and northwest Pacific Ocean. *Geology*, *38*(1), 55–58. https://doi.org/10.1130/g30427.1

van der Meer, D. G., van Hinsbergen, D. J. J., & Spakman, W. (2018). Atlas of the underworld: Slab remnants in the mantle, their sinking history, and a new outlook on lower mantle viscosity. *Tectonophysics*, *723*, 309–448. https://doi.org/10.1016/j.tecto.2017.10.004

van Keken, P. E., Hacker, B. R., Syracuse, E. M., & Abers, G. A. (2011). Subduction factory: 4. Depth-dependent flux of H_2O from subducting slabs worldwide. *Journal of Geophysical Research*, *116*(B1), B01401. https://doi.org/10.1029/2010jb007922

Walter, M. J. (2021). Water transport to the core–mantle boundary. *National Science Review*, *8*(4). https://doi.org/10.1093/nsr/nwab007

Wang, X.-C., Wilde, S. A., Li, Q.-L., & Yang, Y.-N. (2015). Continental flood basalts derived from the hydrous mantle transition zone. *Nature Communications*, *6*(1), 7700. https://doi.org/10.1038/ncomms8700

Wang, Y., & Xu, Y.-G. (2024). Volatiles in the mantle transition zone and their effects on big mantle wedge systems. *National Science Review*, *11*(6). https://doi.org/10.1093/nsr/nwae136

Wirth, R., Vollmer, C., Brenker, F., Matsyuk, S., & Kaminsky, F. (2007). Inclusions of nanocrystalline hydrous aluminium silicate "Phase Egg" in superdeep diamonds from Juina (Mato Grosso State, Brazil). *Earth and Planetary Science Letters*, *259*(3), 384–399. https://doi.org/10.1016/j.epsl.2007.04.041

Xing, K.-C., Wang, F., Teng, F.-Z., Xu, W.-L., Wang, Y.-N., Yang, D.-B., et al. (2024). Potassium isotopic evidence for recycling of surface water into the mantle transition zone. *Nature Geoscience*, *17*(6), 579–585. https://doi.org/10.1038/s41561-024-01452-y

Yan, J., Ballmer, M. D., & Tackley, P. J. (2020). The evolution and distribution of recycled oceanic crust in the Earth's mantle: Insight from geodynamic models. *Earth and Planetary Science Letters*, *537*, 116171. https://doi.org/10.1016/j.epsl.2020.116171

Yang, J., & Faccenda, M. (2020). Intraplate volcanism originating from upwelling hydrous mantle transition zone. *Nature*, *579*(7797), 88–91. https://doi.org/10.1038/s41586-020-2045-y

Young, A., Flament, N., Maloney, K., Williams, S., Matthews, K., Zahirovic, S., & Müller, R. D. (2019). Global kinematics of tectonic plates and subduction zones since the late Paleozoic Era. *Geoscience Frontiers*, *10*(3), 989–1013. https://doi.org/10.1016/j.gsf.2018.05.011

Zhang, H., Egbert, G. D., & Huang, Q. (2022). A relatively dry mantle transition zone revealed by geomagnetic diurnal variations. *Science Advances*, *8*(31), eabo3293. https://doi.org/10.1126/sciadv.abo3293

Zhu, H., Bozdağ, E., Duffy, T. S., & Tromp, J. (2013). Seismic attenuation beneath Europe and the North Atlantic: Implications for water in the mantle. *Earth and Planetary Science Letters*, *381*, 1–11. https://doi.org/10.1016/j.epsl.2013.08.030